

IDPERTURB: Enhancing Variation in Synthetic Face Generation via Angular Perturbations

Fadi Boutros¹, Eduarda Caldeira¹, Tahar Chettaoui¹, Naser Damer^{1,2}

¹Fraunhofer IGD

²Department of Computer Science, TU Darmstadt

Abstract

Synthetic data has emerged as a practical alternative to authentic face datasets for training face recognition (FR) systems, especially as privacy and legal concerns increasingly restrict the use of real biometric data. Recent advances in identity-conditional diffusion models have enabled the generation of photorealistic and identity-consistent face images. However, many of these models suffer from limited intra-class variation, an essential property for training robust and generalizable FR models. In this work, we propose IDPERTURB, a simple yet effective geometric-driven sampling strategy to enhance diversity in synthetic face generation. IDPERTURB perturbs identity embeddings within a constrained angular region of the unit hyper-sphere, producing a diverse set of embeddings without modifying the underlying generative model. Each perturbed embedding serves as a conditioning vector for a pre-trained diffusion model, enabling the synthesis of visually varied yet identity-coherent face images suitable for training generalizable FR systems. Empirical results demonstrate that training FR on datasets generated using IDPERTURB yields improved performance across multiple FR benchmarks, compared to existing synthetic data generation approaches.

1. Introduction

Face recognition (FR) has achieved remarkable progress in recent years, driven by advances in deep neural network architectures, innovations in training objectives, particularly margin-based softmax losses, and the availability of large-scale annotated face datasets [12, 23, 43]. However, acquiring diverse, ethically and legally compliant face datasets remains a significant challenge [14, 42]. Increasing privacy concerns and regulatory constraints surrounding biometric data have led to the withdrawal of several major datasets such as MS-Celeb-1M [15] and VGGFace2 [10], severely limiting access to authentic training data.

These limitations have spurred growing interest in using synthetic data as a scalable and privacy-preserving al-

ternative for training FRs [11, 29, 32]. Recent advances in generative models [21, 22, 36], especially diffusion models (DMs), have enabled the synthesis of photorealistic and identity-consistent face images. Several studies have shown that identity-conditioned DMs can produce synthetic datasets that yield competitive performance compared to real data in downstream FR tasks [5, 24, 33, 45]. However, despite their success in maintaining identity fidelity, many of these models struggle to capture sufficient intra-class variation, an essential factor for training robust and generalizable FR systems.

In this work, we propose IDPERTURB, a simple yet effective sampling strategy for enhancing the diversity of synthetic face datasets. Our method leverages pre-trained identity-conditioned DMs [5] and perturbs identity embeddings within a constrained angular region on the unit hyper-sphere. Rather than using a fixed identity embedding [5, 24, 26, 33] for generation, IDPERTURB creates a set of perturbed embeddings per identity, each serving as a conditioning vector for a unique sample. This results in visually diverse yet semantically coherent outputs. Unlike previous methods that rely on auxiliary labels [45], learned style modules [24], or external models layered over a diffusion backbone [31], IDPERTURB is a fully geometry-driven approach that operates purely in the embedding space and is compatible with pre-trained DMs. By leveraging the geometric structure of identity embeddings, our method introduces diversity while preserving identity semantics to a large extent. Empirically, we demonstrate that IDPERTURB significantly improves intra-class diversity and enhances downstream FR accuracy.

Our main contributions are:

- We propose a geometric method to perturb identity embeddings within a cosine-constrained spherical cap, enabling the generation of images with large variations of the same coherent identity.
- We demonstrate that data generated with IDPERTURB yield superior performance on multiple FR benchmarks, surpassing existing state-of-the-art (SOTA) approaches.

2. Related Work

The rapid progress of deep generative models (DGMs) [21, 22, 36] has enabled the synthesis of photorealistic face images with high identity fidelity and visual diversity. This capability has spurred a surge of interest in using synthetic data to train FR systems [11, 32]. Existing efforts in this domain typically employ generative adversarial networks (GANs) [4, 7, 35] or DMs [24, 45] to generate training datasets for FR.

Early works such as SynFace [35] used DiscoFaceGAN [13] to generate identity-conditioned images and introduced identity mix-up to increase intra-class variability. USynthFace [6] proposed an unsupervised augmentation strategy to simulate diversity from a single synthetic instance. IDNet [25], SFace [4], and SFace2 [8], adopted StyleGAN2-ADA [22] for class-conditional generation. ExFaceGAN [7] disentangled identity attributes in GAN latent space, enabling multi-instance generation from an unconditional model.

DM-based approaches have recently gained attention for their stability and capacity to produce high-fidelity, identity-consistent images. IDiff-Face [5] was among the first to condition DMs on identity embeddings extracted from a pre-trained FR model, injecting noise into the condition during the model training to improve sample diversity. DC-Face [24] introduced dual conditioning with identity and style inputs to control appearance variation. ID³ [45] extended IDiff-Face [5] by incorporating binary attributes as additional conditioning. Arc2Face [33] fine-tuned Stable Diffusion on WebFace42M [50] to generate high-resolution, identity-faithful face images. HyperFace [31] proposed an iterative approach to sample embedding from FR embedding space with large intra-class variations and utilized Arc2Face [33] to generate synthetic data for FR training. GANDiffFace [28] explored hybrid generation by combining GANs with diffusion. The effectiveness of synthetic data for FR has been validated through recent competitions [29, 32]. Winning solutions frequently leveraged diffusion-based synthetic datasets [5, 24], underscoring their superiority in generating diverse and identity-separable samples.

Identity Consistency in DMs: Ensuring identity preservation during generation is a key challenge in diffusion-based synthesis [5, 24, 26, 45], especially for the downstream task of synthetic-based FR. Two main strategies have emerged to address this. The first leverages Classifier-Free Guidance (CFG) [26], where the model is trained both with and without identity conditioning. During inference, predictions are interpolated to modulate conditioning strength. When applied to identity embeddings, CFG effectively improves identity adherence while maintaining sample realism. The second strategy incorporates explicit identity supervision via an additional loss. For instance, DCFace [24]

and ID³ [45] use an identity-preserving loss that minimizes the distance between the identity embedding of the generated image and the conditioning vector. This reinforces identity consistency during the denoising process. Despite the utility of both approaches, CFG-based techniques [26, 33] have demonstrated greater simplicity and effectiveness. Empirical results suggest that synthetic datasets generated with CFG outperform those trained with auxiliary identity losses in downstream recognition tasks [26].

Diversity in Identity-Conditioned Generation: While identity conditioning ensures semantic coherence, it often results in limited intra-class variation—an undesirable property for FR training. To overcome this, DC-Face [24] supplements the identity condition with a learned style embedding, allowing stylistic diversity across samples. ID³ [45] introduces binary attributes as additional conditions, enabling explicit control of intra-class variation. IDiff-Face [5] applies dropout to the identity context during training to encourage generalization. HyperFace [31] proposed an iterative approach to optimize intra-class variation for generating synthetic identities from a spherical space. UIFace [26] employs a two-phase sampling scheme where the model generates early steps unconditionally and incorporates the identity condition only in later denoising steps, allowing more stochastic variations.

While prior work has significantly advanced synthetic face generation for FR, balancing identity preservation and visual diversity, many approaches depend on auxiliary labels [45], network modifications [24], or iterative learnable approaches for context sampling [31]. In contrast, our method leverages the geometry of the identity embedding space to introduce variations via angular sampling, enhancing diversity without compromising identity fidelity. This simple strategy enables the generation of diverse samples from pre-trained DMs.

3. Methodology

This section presents our proposed method, IDPERTURB, a sampling strategy designed to enhance intra-class variation in synthetic face generation. Our approach operates directly in the identity-condition embedding space of a pre-trained identity-conditional DM. The core idea is to perturb the fixed identity embedding within a constrained angular region, defined as a d -dimensional cone, thus generating samples that are diverse yet, to a large degree, identity-consistent. Given a pre-trained DM conditioned on identity features (i.e., embeddings extracted by a FR model), IDPERTURB perturbs the conditioning vector by controlling its angular distance from the original embedding. This process yields a set of perturbed identity embeddings, which are then used as input to the DM to synthesize face images. We first provide in this section preliminaries on DM, followed by our proposed IDPERTURB.

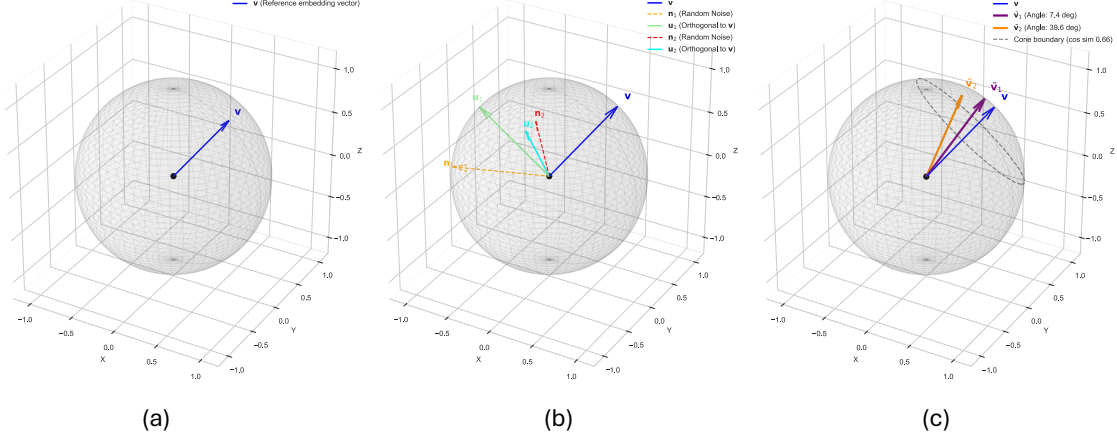


Figure 1. Identity perturbation in the embedding space. (a) a normalized reference embedding $\mathbf{v} \in \mathbb{R}^3$. (b) random $\mathbf{n}_1, \mathbf{n}_2 \sim \mathcal{N}(0, \mathbf{I})$ sampled and projected onto the hyperplane orthogonal to \mathbf{v} , resulting in \mathbf{u}_1 and \mathbf{u}_2 (Equation 4). (c) perturbed identity vector $\tilde{\mathbf{v}}_1$ and $\tilde{\mathbf{v}}_2$ with different angle to \mathbf{v} are constructed (Equation 5). Note, this figure is not manually plotted, rather, using a Python script corresponding to Algorithm 1. The cone boundary, dashed circumference in (c), is defined by the lower bound lb is 0.66, and \mathbf{n}_1 and \mathbf{n}_2 are sampled on the fly to illustrate a real scenario. For visualization purposes, we set the number of dimensions to 3, $\mathbf{v} \in \mathbb{R}^3$.

3.1. Latent DM Preliminaries

Latent Diffusion Models (LDMs) [36] improve the efficiency of diffusion-based image generation by operating in a compressed latent space rather than directly in pixel space. Given a training image $\mathbf{x}_0 \in \mathbb{R}^{H \times W \times C}$, a pre-trained encoder $\mathcal{E} : \mathbb{R}^{H \times W \times C} \rightarrow \mathbb{R}^d$ maps it to a latent representation $\mathbf{z}_0 = \mathcal{E}(\mathbf{x}_0)$.

To learn the generative process, LDMs adopt the denoising diffusion probabilistic model (DDPM) framework [18], where the latent code \mathbf{z}_0 is gradually perturbed by Gaussian noise over T discrete timesteps:

$$q(\mathbf{z}_t | \mathbf{z}_{t-1}) = \mathcal{N}(\mathbf{z}_t; \sqrt{1 - \beta_t} \mathbf{z}_{t-1}, \beta_t \mathbf{I}), \quad (1)$$

where $\{\beta_t\}_{t=1}^T$ is a predefined variance schedule. After sufficient noising steps, the latent \mathbf{z}_T approximates an isotropic Gaussian distribution, i.e., $\mathbf{z}_T \sim \mathcal{N}(0, \mathbf{I})$.

The reverse process is modeled by a neural network θ , typically implemented as a U-Net [36], which is trained to denoise the latent variable by predicting the noise component added at each step. The network takes as input the noisy latent \mathbf{z}_t , the timestep t , and an optional conditioning signal $\mathbf{v} \in \mathbb{R}^d$, such as an identity embedding. The reverse process is thus formulated as:

$$p_\theta(\mathbf{z}_{t-1} | \mathbf{z}_t, \mathbf{v}) = \mathcal{N}(\mathbf{z}_{t-1}; \mu_\theta(\mathbf{z}_t, t, \mathbf{v}), \Sigma_\theta(\mathbf{z}_t, t, \mathbf{v})). \quad (2)$$

In identity-conditional LDMs [5, 26, 45], the identity embedding \mathbf{v} , typically extracted using a pre-trained FR model, is injected into the U-Net via cross-attention layers [36]. This mechanism projects the identity context into the intermediate feature representations of the denoising network, allowing the generative process to dynamically adapt to the given identity [5, 36]. Note that the condition is dropped (i.e, condition is set to zeros) with probability $P = 20$ during the training to enable unconditional

sampling [26]. After the denoising trajectory is complete, the final latent $\hat{\mathbf{z}}_0$ is passed through a pre-trained decoder $\mathcal{D} : \mathbb{R}^d \rightarrow \mathbb{R}^{H \times W \times C}$, to reconstruct image $\hat{\mathbf{x}}_0 = \mathcal{D}(\hat{\mathbf{z}}_0)$.

To generate identity-conditioned synthetic data using a pre-trained LDM, the common approach [5, 24, 26, 45] is to first sample an image \mathbf{x}' using an unconditional generative process (i.e., conditioning input of zeros). A feature representation $\mathbf{v}' = f(\mathbf{x}')$ is then extracted using a pre-trained FR model f . This embedding \mathbf{v}' serves as the identity condition to generate new samples from the conditional LDM by fixing \mathbf{v}' and varying the initial noise seed, \mathbf{z}_T [5, 26].

Classifier-Free Guidance (CFG): CFG [17] can be utilized to amplify the effect of the identity condition during generation [26]. CFG has proven effective across a range of conditional generation tasks, including both image- and text-guided scenarios [2, 26, 44]. At inference time, the predicted noise is interpolated between the conditioned and unconditioned outputs as follows:

$$\hat{\epsilon} = (1 + \omega) \hat{\epsilon}_\theta(\mathbf{z}_t, t, \mathbf{v}') - \omega \hat{\epsilon}_\theta(\mathbf{z}_t, t), \quad (3)$$

where ω is the guidance strength parameter. Increasing ω enhances the model's adherence to the identity condition, promoting better identity consistency in the generated data.

3.2. Data Generation via Angular Sampling

For identity-conditioned generation, particularly in applications such as facial synthesis for training FRs, the generated data must simultaneously fulfill two critical objectives: maintaining high identity consistency across samples of the same identity and exhibiting realistic intra-identity variation. These properties are paramount for the effective utilization of synthetic data in downstream FR tasks. Existing methodologies often rely on auxiliary modules [24, 45] or employ complex learned sampling strategies on top of generative models [31] to introduce diversity. In contrast, we

introduce Angular Sampling, a novel geometric approach designed to stochastically perturb the conditioning identity vector in a semantically coherent manner, without requiring architectural modifications of identity-conditional DMs.

Assumption We assume that the pre-trained DM, conditioned on identity embeddings, generates, to a large extent, identity-consistent samples, a property we empirically verify in our experiments. There is no additional condition, e.g., binary attribute conditions or style conditions from a style bank. This assumption is essential to disentangle the source of intra-class variations in this work.

Angular Sampling Formulation The key idea of our approach is to perturb the identity condition \mathbf{v} geometrically within the identity embedding space. This preserves, to a large degree, semantic identity while introducing diversity without modifying the base LDM.

Let $\mathbf{v} \in \mathbb{R}^d$ be a unit-norm identity embedding extracted from an FR model. Our goal is to sample a perturbed embedding $\tilde{\mathbf{v}}$ such that the angular separation, $\angle(\mathbf{v}, \tilde{\mathbf{v}})$, is constrained within a d -dimensional cone defined by cosine similarity bounds $[\mathbf{lb}, 1] \subset [0, 1]$, where \mathbf{lb} is the lower bound. The procedure for generating $\tilde{\mathbf{v}}$ for each synthetic image is illustrated in Figure 1 and is defined as follows. To generate a set of images corresponding to identity condition \mathbf{v} , we first uniformly sample a target cosine similarity $s \sim \mathcal{U}[\mathbf{lb}, 1]$, corresponding to angle $\theta = \cos^{-1}(s)$. Then, we sample random noise $\mathbf{n} \sim \mathcal{N}(0, \mathbf{I})$ where $\mathbf{n} \in \mathbb{R}^d$. We then project \mathbf{n} onto the hyperplane orthogonal to \mathbf{v} by subtracting the component of \mathbf{n} in the direction of \mathbf{v} :

$$\mathbf{u} = \frac{\mathbf{n} - (\mathbf{n} \cdot \mathbf{v})\mathbf{v}}{\|\mathbf{n} - (\mathbf{n} \cdot \mathbf{v})\mathbf{v}\|}. \quad (4)$$

This projection removes the contribution of \mathbf{v} from \mathbf{n} , ensuring that \mathbf{u} is orthogonal to \mathbf{v} . The normalization step guarantees that \mathbf{u} has unit norm. Geometrically, \mathbf{u} lies on the unit tangent hyper-sphere at \mathbf{v} , and together with \mathbf{v} , they span a \mathbb{R}^d subspace in which angular sampling is performed. Finally, we construct the perturbed identity:

$$\tilde{\mathbf{v}} = \cos(\theta) \cdot \mathbf{v} + \sin(\theta) \cdot \mathbf{u}, \quad (5)$$

where θ is the target angle sampled via $\theta = \cos^{-1}(s)$, with $s \sim \mathcal{U}[\mathbf{lb}, 1]$. Since v and u are orthonormal, $\|\tilde{\mathbf{v}}\| = 1$ and $\langle \tilde{\mathbf{v}}, \mathbf{v} \rangle = \cos(\theta)$ hold, providing strict control over the perturbation magnitude while preserving identity semantics.

Properties The constructed perturbed embedding $\tilde{\mathbf{v}}$ satisfies the following geometric and semantic guarantees:

- **Norm Preservation:** $\|\tilde{\mathbf{v}}\|^2 = \cos^2(\theta) + \sin^2(\theta) = 1$
- **Angle Control:** $\langle \tilde{\mathbf{v}}, \mathbf{v} \rangle = \cos(\theta) = s$
- $\theta = 0$: $\tilde{\mathbf{v}}$ and \mathbf{v} are identical. **Proof:** $\|\tilde{\mathbf{v}}\| = \|\mathbf{v}\| = 1$, $\cos(\theta) = 1$, $\sin(\theta) = 0$, $\tilde{\mathbf{v}} = 1 \cdot \mathbf{v} + 0 \cdot \mathbf{u}$,

Theoretical details and justifications are provided in the supplementary material.

Lower Bound Constraint The parameter \mathbf{lb} (lower bound) delineates the permissible range for the cosine similarity between the original identity embedding \mathbf{v} and its perturbed counterpart $\tilde{\mathbf{v}}$. Geometrically, this defines a spherical cap around \mathbf{v} . A smaller value of \mathbf{lb} facilitates greater variation in the generated samples, whereas values approaching 1 enforce stricter identity faithfulness. Notably, when $\mathbf{lb} = 1$, \mathbf{v} and $\tilde{\mathbf{v}}$ are identical, resulting in no perturbation.

Avoiding Identity Overlap Consider a set of reference synthetic identity embedding \mathbf{V} extracted using a pre-trained FR model from a set of reference images \mathbf{X} , i.e., synthetic images generated using an unconditional generative model [5, 26]. To mitigate the risk of the perturbed vector $\tilde{\mathbf{v}}$ from $\mathbf{v}_i \in \mathbf{V}$ becoming semantically closer to any other distinct identities, $\mathbf{v}_j \in \mathbf{V}$, than to its intended identity \mathbf{v}_i , we dynamically adjust the lower bound \mathbf{lb} :

$$\mathbf{lb} \leftarrow \max \left(\mathbf{lb}, \max_{j \neq i} \cos \left(\frac{\angle(\mathbf{v}_i, \mathbf{v}_j)}{2} \right) \right), \quad (6)$$

where dividing the angle that separates \mathbf{v}_i and \mathbf{v}_j in half ensures that $\tilde{\mathbf{v}}$ lays closer to \mathbf{v}_i than \mathbf{v}_j ($\angle(\tilde{\mathbf{v}}, \mathbf{v}_i) \leq \angle(\tilde{\mathbf{v}}, \mathbf{v}_j)$).

Data Generation For each synthetic identity embedding $\mathbf{v} \in \mathbf{V}$, we apply the angular sampling method described in Algorithm 1 to generate a set of K perturbed identity embeddings $\{\tilde{\mathbf{v}}_k\}_{k=1}^K$. These perturbed embeddings serve as identity-conditioning inputs to a pre-trained LDM. Specifically, for each $\tilde{\mathbf{v}}_k$, we sample a noise latent $\mathbf{z}_{T_k} \sim \mathcal{N}(0, \mathbf{I})$ and apply the reverse diffusion process (Equation 2): $\mathbf{z}_{0_k} = \text{LDM}(\mathbf{z}_{T_k}, \tilde{\mathbf{v}}_k)$, where the identity condition $\tilde{\mathbf{v}}_k$ remains fixed across all timesteps $t = T, \dots, 1$. The final synthetic image $\hat{\mathbf{x}}_k$ is obtained by decoding the denoised latent using the LDM decoder D : $\hat{\mathbf{x}}_k = D(\mathbf{z}_{0_k})$. By repeating this process for multiple $\tilde{\mathbf{v}}_k$, we construct a set of diverse yet identity-coherent face images $\{\hat{\mathbf{x}}_k\}_{k=1}^K$ associated with a single synthetic identity \mathbf{v} . This set can then be used as training data for FR models.

Algorithm 1 Angular Sampling Algorithm

Require: Reference identity embedding $\mathbf{v}_i \in \mathbf{V}$, lower bound

$\mathbf{lb} \in [0, 1]$, number of samples per identity K

Ensure: Set of perturbed identity vectors $\{\tilde{\mathbf{v}}_{i_k}\}_{k=1}^K$

- 1: Normalize $\mathbf{v}_i \leftarrow \frac{\mathbf{v}_i}{\|\mathbf{v}_i\|}$
 - 2: $\mathbf{lb} \leftarrow \max \left(\mathbf{lb}, \max_{j \neq i} \cos \left(\frac{\angle(\mathbf{v}_i, \mathbf{v}_j)}{2} \right) \right)$, $\mathbf{v}_j \in \mathbf{V}$
 - 3: **for** $k = 1$ to K **do**
 - 4: Sample $s \sim \mathcal{U}[\mathbf{lb}, 1]$
 - 5: Compute $\theta \leftarrow \cos^{-1}(s)$
 - 6: Sample noise $\mathbf{n} \sim \mathcal{N}(0, \mathbf{I}_d)$
 - 7: Project: $\mathbf{u} \leftarrow \frac{\mathbf{n} - (\mathbf{n} \cdot \mathbf{v}_i)\mathbf{v}_i}{\|\mathbf{n} - (\mathbf{n} \cdot \mathbf{v}_i)\mathbf{v}_i\|}$
 - 8: Compute perturbed vector: $\tilde{\mathbf{v}}_{i_k} \leftarrow \cos(\theta)\mathbf{v}_i + \sin(\theta)\mathbf{u}$
 - 9: **end for**
 - 10: **return** $\{\tilde{\mathbf{v}}_{i_k}\}_{k=1}^K$
-

Table 1. Identity separability of synthetic datasets (left side) and verification accuracy (%) of FR models trained on those datasets (right side). The data was generated by varying the d -dimensional cone boundary $l_b \in [0.4, 0.9]$ on two baseline LDM models: IDiff-Face trained on FFHQ and IDiff-Face trained on C-WF. The FR evaluation results on 5 benchmarks demonstrated that IDPERTURB achieves consistent and superior performance over the baselines across all FR benchmarks. The results of the first row were obtained from authentic C-WF. The corresponding histograms of score distributions are provided in the supplementary material.

		Identity-Separability of Training Data						FR Verification						
Data Sampling Method	l _b	Operation Metrics		Score Distributions				Verification Benchmarks						
		EER ↓	FMR100 ↓	genuine	imposter	FDR ↑	LFW ↑	AgeDB-30 ↑	CFP-FP ↑	CALFW ↑	CP-LFW ↑	Average ↑		
		G-mean	G-std	I-mean	I-std									
C-WF [5, 46]	-	0.076	0.092	0.536	0.215	0.003	0.070	5.541	99.55	94.55	95.31	93.78	89.95	94.63
Baseline (FFHQ)	-	0.005	0.004	0.509	0.104	0.023	0.081	13.680	97.60	84.10	83.36	89.08	78.77	86.58
	0.9	0.010	0.011	0.448	0.108	0.023	0.060	11.817	98.05	86.78	83.79	89.92	79.02	87.51
	0.8	0.023	0.038	0.390	0.116	0.023	0.060	7.961	98.22	87.42	84.26	90.65	81.20	88.35
	0.7	0.047	0.102	0.337	0.124	0.022	0.060	5.236	98.47	88.25	84.50	91.18	81.27	88.73
	0.6	0.082	0.208	0.288	0.130	0.023	0.060	3.422	98.43	88.77	83.61	91.07	80.80	88.54
	0.5	0.124	0.332	0.245	0.133	0.023	0.060	2.316	98.55	88.85	84.27	91.42	80.85	88.79
	0.4	0.171	0.457	0.208	0.134	0.023	0.060	1.588	98.48	88.70	83.00	91.57	76.13	87.58
Baseline (C-WF)	-	0.003	0.001	0.670	0.107	0.010	0.060	29.116	98.75	88.85	91.61	90.90	86.15	91.25
	0.9	0.006	0.005	0.580	0.121	0.010	0.061	17.728	99.13	91.30	93.00	92.18	87.80	92.68
	0.8	0.014	0.016	0.494	0.138	0.009	0.059	10.471	99.30	92.13	93.73	93.07	88.30	93.31
	0.7	0.032	0.053	0.412	0.153	0.008	0.059	6.083	99.28	92.37	93.80	93.38	88.37	93.44
	0.6	0.063	0.134	0.338	0.162	0.008	0.059	3.664	99.40	93.20	93.61	93.50	88.37	93.62
	0.5	0.104	0.253	0.278	0.166	0.008	0.059	2.363	99.27	93.25	93.67	93.58	88.02	93.56
	0.4	0.152	0.254	0.228	0.164	0.008	0.059	1.599	99.28	93.25	93.06	93.62	87.62	93.36

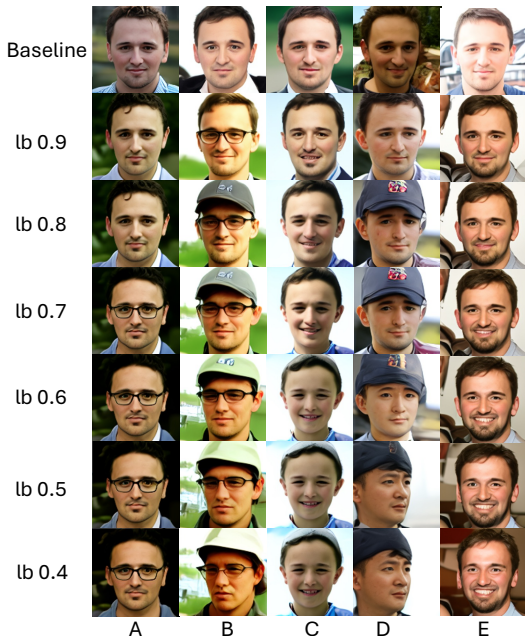


Figure 2. Effect of IDPERTURB (via lower bound l_b) on image diversity. The first row varies only the noise seed with fixed condition \mathbf{v} , subsequent rows use perturbed identity embeddings $\tilde{\mathbf{v}}$ from \mathbf{v} with decreasing l_b (0.9 to 0.4). Lower l_b values increase angular deviation, enhancing intra-class variation. Note that using low l_b of e.g., 0.4, the identity of some samples could be less consistent, which is also quantified by high EER in Table 1.

4. Experimental Setup

Baseline DMs We evaluate our approach on top of two instances of pre-trained IDiff-Face [5] with a contextual partial dropout of 25% as the base DM. IDiff-Face is a conditional LDM trained on the latent space of a pre-trained Auto-Encoder [36] and conditioned on identity contexts, i.e., embeddings from a pre-trained FR. The first instance is trained on the Flickr-Faces-HQ (FFHQ) dataset [21], fol-

lowing [5, 41], and it was publicly released¹ by [5]. The second instance of IDiff-Face [5] was trained on Casia-WebFace (C-WF), and the pre-trained model was publicly released² by [26]. The choice of model trained on FFHQ [5, 41], and C-WF [23, 26] is to provide comparable results with SOTA.

Synthetic data generation We utilized synthetic reference embeddings publicly released² by UFace [26]. It is based on generating a set of reference images using unconditional IDiff-Face [5]. Then, feature representations were extracted using a pre-trained FR [3]. Subsequently, we utilized our IDPERTURB described in Algo. 1 to generate 50 images per identity. We generated 20 datasets using IDiff-Face [5], each with different l_b of 0.9, 0.8, 0.7, 0.6, 0.5 and 0.4 as well as using different baseline DMs and ω . In the inference phase, we utilized a Denoising Diffusion Implicit Model (DDIM) [40] with 50 steps, following [26] with a fixed random seed of 1337, ensuring consistent generation across different runs. IDPERTURB induces negligible computation overhead to DM sampling with an extra 0.01 seconds to perturb 1 identity 50 times on M3 CPU processor.

Identity-Separability Evaluation We evaluate the identity-separability of synthetic data generated with IDPERTURB and compare it to the case where data is generated without the identity perturbation. These evaluations are reported as FMR100, which is the lowest false non-match rate (FNMR) for a false match rate (FMR) $\leq 1.0\%$, along with the Equal Error Rate (EER), as in [4, 5]. The inter-class separability and intra-class compactness are evaluated by reporting the genuine and imposter means (G-mean and I-mean) and standard deviation (G-STD and I-STD), respectively. Additionally, we report the Fisher discriminant ratio (FDR) [34] to quantify the separability of genuine and im-

¹<https://github.com/fdbtrs/IDiff-Face>

²<https://github.com/Tencent/TFace/>

postor scores [4, 5]. We used a pre-trained ResNet100 [16] with ElasticFace [3] on MS1MV2 [12, 15] to extract the feature representations needed for these evaluations.

Intra-Class Diversity and Consistency To quantify intra-class diversity induced by IDPERTURB, we first analyze three complementary metrics, age deviation, facial expression variation, and head-pose variation, across images generated under different cone boundaries. Age variation was estimated using a pre-trained age estimation model [20], measuring the entropy of predicted ages within each identity. Facial expression variation was estimated using a pretrained estimator [39], measuring the entropy of predicted expression within each identity. Head-pose diversity was assessed using a pretrained head-pose regressor [37] by computing the standard deviation (STD) of yaw–pitch–roll angles per identity. Intra-Class diversity was measured using the Learned Perceptual Image Patch Similarity (LPIPS) [47] computed between intra-identity image pairs to quantify perceptual variation in appearance:

$$D_{intra} = \frac{1}{C} \sum_{i=1}^C \frac{2}{M_i(M_i - 1)} \sum_{j=1}^{M_i-1} \sum_{l=j+1}^{M_i} \left(\text{LPIPS}(x_j^{(i)}, x_l^{(i)}) \right), \quad (7)$$

where C is number of classes, M_i is number of samples per class i and LPIPS [47] is perceptual similarity metric.

We reported the intra-class consistency by measuring the ratio of feature $f(x_j^{(i)})$ of sample j of class i being close to its class center μ_i . Intra-class consistency is defined, following [23], as:

$$C_{intra} = \frac{1}{C} \sum_{i=1}^C \frac{1}{M_i} \sum_{j=1}^{M_i} \mathbb{I} \left(\text{sim}(f(x_j^{(i)}), \mu_i) \geq r \right), \quad (8)$$

where the class center $\mu_i = \frac{1}{M_i} \sum_{j=1}^{M_i} f(x_j^{(i)})$, C is number of classes, M_i is number of samples per class i , $f(x_j^{(i)})$ is feature embedding of the j -th sample in class i extracted from [3], $\text{sim}(\cdot, \cdot)$ is cosine similarity, r is similarity threshold of value 0.3 [23] and $\mathbb{I}(\cdot)$ is the indicator function that returns 1 if the condition is true and 0 otherwise.

FR Training Setup We utilized ResNet50 [16] as a network architecture with CosFace loss [43] to train FR on our synthetic datasets, following [5, 7, 26, 41]. We set the mini-batch size to 512 and train with a Stochastic Gradient Descent (SGD) optimizer for 34 epochs, setting the momentum to 0.9 and the weight decay to $5e-4$, following [5, 7, 41]. Initial learning rate is set to 0.1 and is reduced by a factor of 0.1 at epochs 22, 28 and 32. The margin penalty of CosFace loss was set to 0.35 and the scale factor to 64 [43].

Evaluation Benchmarks We report FR evaluation results, following [5, 7, 23, 26], as the verification accuracy on five benchmarks, Labeled Faces in the Wild LFW [19],

AgeDb-30 [30], Cross-Age LFW (CA-LFW) [49], Celebrities in Frontal-Profile in the Wild (CFP-FP) [38], and Cross-Pose LFW (CP-LFW) [48], following their official evaluation protocol. Additionally, we evaluated on the large-scale IARPA Janus Benchmark-C (IJB-C) [27]. We used the official 1:1 mixed verification protocol and reported the verification performance as True Acceptance Rates (TAR) at False Acceptance Rates (FAR) of $1e-4$ and $1e-5$.

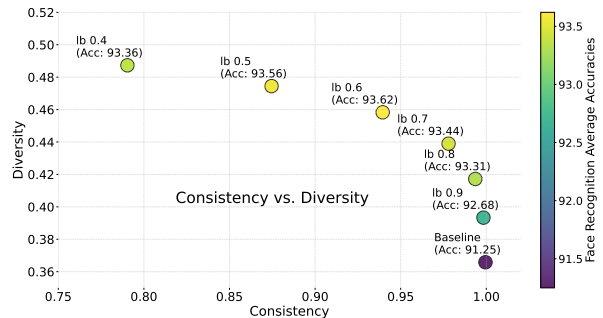


Figure 3. FR average accuracies (as in Table 1) with respect to the intra-class consistency and diversity of baseline (C-WF) and IDPERTURB of $lb \in [0.4, 0.5, 0.6, 0.7, 0.8, 0.9]$.

5. Results

We first evaluate the impact of IDPERTURB on identity separability and intra-class diversity. We then assess the effectiveness of synthetic data generated using IDPERTURB as a FR training dataset across multiple FR benchmarks, reporting improvements compared to recent SOTA approaches.

5.1. Impact of Identity Perturbation

We begin by analyzing the effect of the d -dimensional cone boundary, defined by the lower bound hyperparameter lb , on identity-separability and downstream verification performance. Specifically, we generate datasets using different values of $lb \in \{0.9, 0.8, 0.7, 0.6, 0.5, 0.4\}$ on top of two pre-trained DMs: IDiff-Face trained on FFHQ and IDiff-Face trained on C-WF. These are compared against the baseline setting with no perturbation ($lb = 1.0$). In these experiments, we fix the $\omega = 1$ of CFG, following [26].

Identity Separability Analysis We analyze the identity separability of the generated datasets under varying levels of lb , as reported in the left part of Table 1. The baseline (unperturbed) yields high identity separability, achieving an EER of 0.005, which is substantially lower than the 0.076 reported for authentic C-WF. This confirms that identity-conditioned DMs with CFG generate identity-consistent samples, supporting our statement in Methodology 3. However, this high separability also suggests that intra-class variation in the baseline synthetic data is limited, making the samples less challenging and potentially suboptimal for training robust FR models. When applying IDPERTURB, we observe that decreasing lb results in an expected

increase in EER and a decrease in the mean of genuine scores. This trend reflects increased intra-class diversity, as the generated samples become more challenging. Importantly, even with strong perturbations, identity separability remains largely intact (e.g., $lb = 0.6$ yielding $EER = 0.082$ vs. 0.076 reported for the authentic dataset C-WF), indicating that identity consistency is not severely compromised.

Table 2. Intra-class diversity and consistency on top of the Baseline(C-WF) reported as age entropy, facial expression (Exp.) entropy, head-pose STD, D_{intra} and C_{intra} . Higher age and expression entropy, and pose STD, and D_{intra} indicate greater intra-class diversity. The first row shows authentic C-WF results. Baseline (C-WF) is generated from the DM without IDPERTURB.

Dataset	lb	Attributes				D-Intra	C-Intra	FR-Perf.	
		Age \uparrow	Yaw	Pose \uparrow	Roll				
C-WF	-	0.354	23.479	9.069	5.154	0.589	0.423	0.948	94.63
Baseline (C-WF)	-	0.283	18.881	7.992	3.230	0.429	0.366	0.999	91.25
IDPERTURB	0.9	0.325	19.907	8.384	3.606	0.492	0.393	0.998	92.68
	0.8	0.369	20.899	8.727	4.029	0.538	0.417	0.994	93.31
	0.7	0.416	21.816	9.117	4.551	0.574	0.439	0.978	93.44
	0.6	0.461	22.735	9.467	5.124	0.603	0.458	0.939	93.62
	0.5	0.501	23.611	9.724	5.602	0.621	0.474	0.875	93.56
	0.4	0.538	24.279	9.957	6.040	0.636	0.487	0.790	93.36

Intra-Class Diversity and Consistency To further evaluate intra-class diversity and consistency, we report in Table 2 the age entropy, facial expression entropy, STD of head-pose, intra-class perceptual diversity, and intra-class consistency. We observe that decreasing lb from 0.9 to 0.4 leads to a gradual increase in intra-class age and facial expression deviation (see also Figure 2 C: baseline vs. lb 0.7), suggesting that angular perturbation successfully introduces naturalistic expression and age-related cues, without compromising identity coherence. Similar observations can be made on head-pose, where the pose variation increases consistently with wider perturbation bounds, reaching up to STD of 23.611° yaw deviation at $lb = 0.5$. This indicates that IDPERTURB implicitly encourages pose diversification even though it operates solely in the identity-embedding space (see also Figure 2 B and D: baseline vs. lb 0.5). As expected, the intra-class diversity (D_{intra}) increases monotonically with decreasing lb , confirming that IDPERTURB effectively expands the perceptual manifold of each identity Table 2. A tradeoff between D_{intra} and C_{intra} is illustrated in Figure 3 with FR performances of models trained on IDPERTURB with the best performance achieved by IDPERTURB ($lb = 0.6$), see Table 1 for details evaluations.

FR Verification Performance The right side of Table 1 presents the verification accuracy of FR models trained on datasets from IDPERTURB. Across all benchmarks, IDPERTURB consistently outperforms baseline models trained on data generated without identity perturbation. For the baseline LDM model trained on FFHQ, IDPERTURB achieves a peak average accuracy of 88.79% at $lb = 0.5$, compared to 86.58% for the baseline ($lb = 1.0$). Notably, all tested values of $lb \in [0.9, 0.4]$ outperform the baseline. Similarly, for the LDM model trained on C-WF, ID-

PERTURB improves the average accuracy from 91.25% to 93.62% , with performance increasing as lb decreases, until it peaks for $lb = 0.6$. In all the following experiments, we fix Our method generalizes well across challenging benchmarks such as CALFW, AgeDB-30, and CP-LFW, which involve cross-pose and cross-age variations. Additional results of FR performances using different loss functions and network architectures are provided in the supplementary materials.

5.2. Impact of CFG Strength

To further understand the interaction between guidance strength and the model’s adherence to the identity condition, we perform an ablation study over the CFG scale ω in Equation 3. This study was performed on the C-FW dataset and, thus, we fixed the d -dimensional cone boundary based on the best performing setting, $lb = 0.6$ (Table 1), while varying $\omega \in \{0, 1, 2, 3, 4, 5\}$. As shown in Table 3, increasing ω improves the model’s adherence to the identity condition v , as evidenced by reduced EER. However, stronger guidance also restricts sample diversity, resulting in reduced FR accuracy when training on highly guided synthetic datasets. The best verification performance is achieved at moderate guidance values $\omega = 1$ or $\omega = 2$. In summary, these results highlight the importance of a trade-off between identity consistency, achieved via CFG, and intra-class variation, introduced through IDPERTURB. The combination of both is critical for generating effective training data for FR.

5.3. Comparison with State-of-the-Art

We compare IDPERTURB with SOTA synthetic data generation methods, including digital rendering, GAN-based and DM-based approaches. Compared to GAN or digital rendering (e.g., DigiFace-1M, IDNet, SFace, SFace2+), IDPERTURB achieves superior performance across all benchmarks, highlighting the advantages of DMs, especially when combined with geometry-aware identity sampling. Among DM-based methods trained under comparable data regimes (FFHQ with 70K images) and by generating 0.5M images for FR training, IDPERTURB outperforms ID³ and IDiff-Face on LFW, AgeDB, CALFW, and CP-LFW, and achieves nearly competitive performance on CFP-FP. When the DM training data is scaled up (e.g., C-WF with 0.49M or WebFace4M (WF4M) with 4M images), IDPERTURB remains highly competitive, ranking first on LFW, AgeDB, and CALFW, and second on CFP-FP and CP-LFW, slightly behind UIFace. Overall, considering the average performance across five benchmarks, IDPERTURB achieves the highest average verification accuracy of 93.62% , outperforming all compared synthetic-based FR systems under equivalent evaluation conditions. Similar observation can be made on challenging IJB-C, where IDPERTURB outperforms other competitors. In comparison to FR trained on authentic C-WF (average accuracy of 94.63%), our syn-

Table 3. Identity separability of synthetic datasets (left side) and verification accuracy (%) of FR models trained on those datasets (right side). We compare IDPERTURB-based synthetic datasets (generated using base DM trained on C-WF with varying scale $\omega \in [0, 5]$ values and fixed d -dimensional cone boundary $\mathbf{Ib} = 0.6$).

		Identity-Separability of Training Data							FR Verification					
Data Sampling Method	Scale	Operation Metrics		Score Distributions					Verification Benchmarks					
		EER ↓	FMR100 ↓	genuine	imposter	G-mean	G-std	I-mean	I-std	FDR ↑	LFW ↑	AgeDB-30 ↑	CFP-FP ↑	CALFW ↑
IDPERTURB	0	0.162	0.427	0.185	0.124	0.006	0.058	1.718	99.25	92.58	92.31	93.53	87.17	92.97
	1	0.063	0.134	0.338	0.162	0.008	0.059	3.664	99.40	93.20	93.61	93.50	88.37	93.62
	2	0.043	0.079	0.394	0.168	0.012	0.060	4.611	99.33	93.33	93.56	93.42	88.53	93.63
	3	0.036	0.064	0.414	0.169	0.014	0.060	4.987	99.22	92.83	92.66	93.20	87.83	93.15
	4	0.034	0.060	0.421	0.168	0.017	0.061	5.105	99.07	91.90	92.04	92.70	87.42	92.63
	5	0.034	0.059	0.424	0.168	0.018	0.061	5.136	98.93	91.90	91.63	92.42	87.20	92.42

Table 4. FR verification accuracies of IDPERTURB and SOTA on small (LFW, AgeDB-30, CFP-FP, CA-LFW and CP-LFW) and large-scale IJB-C benchmarks. We highlight the datasets used to train generative models, FFHQ [21] (70k images) vs. C-WF [46] (0.49M images) vs. WebFace4M (WF4M) [50] (4M images) Under the same settings, i.e., DGM trained on large C-WF, IDPERTURB outperformed all competitors on the considered evaluation benchmarks with an average accuracy of 93.62%. The results marked with a star (*) are reproduced in this work, as there was no publicly released FR model. Some of the previous works did not release their pre-trained model and their generated data and there were no reported results on the large-scale IJB-C [27]. The first row presents the results achieved by authentic C-WF, which are provided as a reference. Best results for each DM setup are shown in **bold**, and second-best ones are underlined.

Method	Data Generation	DGMs Train Dataset	#imgs (IDs × imgs/ID)	LFW	AgeDB	CFP-FP	CA-LFW	CP-LFW	Avg	IJB-C	
										10 ⁻⁵	10 ⁻⁴
C-WF [5, 46]	Authentic	-	0.49M (~10.5k × 47)	99.55	94.55	95.31	93.78	89.95	94.63	93.96	96.05
DigiFace [1] WACV'22	Digital Rendering	-	0.5M(10k × 50)	95.40	76.97	87.40	78.62	78.87	83.45	-	-
DigiFace [1]* WACV'22		-	0.5M(10k × 50)	91.15	74.00	82.93	75.30	73.40	79.36	30.01	44.78
DigiFace [1] WACV'22		-	1.2M(10k × 72 + 100k × 5)	96.17	81.10	89.81	82.55	82.23	86.37	-	-
IDnet [25] CVPRW'23	GAN-Based	C-WF	0.5M(10.5k × 50)	92.58	73.53	75.40	79.90	74.25	79.13	38.85	53.25
SFace [4] IJCV'22		C-WF	0.63M(10.5k × 60)	91.87	71.68	73.86	77.93	73.20	77.71	12.70	19.87
SFace2+ [8] TBIOM'24		C-WF	0.63M(10.5k × 60)	95.60	77.37	77.11	83.40	74.60	81.62	0.85	5.36
SynFace [35] ICCV'21		FFHQ	0.5M(10k × 50)	88.98	-	-	-	-	-	-	-
SynFace (w/IM) [35] ICCV'21		FFHQ	0.5M(10k × 50)	91.93	61.63	75.03	74.73	70.43	74.75	-	-
USynthFace [6] FG'23		FFHQ	0.4M(400k × 1)	92.23	71.62	78.56	77.05	72.03	78.30	-	-
ExFaceGAN(Con) [7] IJCV'23		FFHQ	0.5M(10k × 50)	93.50	78.92	73.84	82.98	71.60	80.17	12.92	43.28
ID ³ [45] NeurIPS'24		FFHQ	0.5M(10k × 50)	97.28	83.78	85.00	89.30	77.13	86.50	-	-
IDDiff-Face [5] ICCV'24		FFHQ	0.5M(10k × 50)	<u>98.00</u>	86.43	85.47	90.65	80.45	<u>88.20</u>	20.60	62.60
NegFaceDiff [9] ICCV-W'25		FFHQ	0.5M(10k × 50)	97.60	<u>86.53</u>	<u>85.33</u>	<u>90.28</u>	<u>80.73</u>	<u>88.10</u>	58.09	<u>73.93</u>
IDPERTURB (Ours)	FFHQ	0.5M(10k × 50)	98.55	88.85	84.27	91.42	80.85	88.79	<u>37.88</u>	74.49	
Arc2Face [33] ECCV'24	Diffusion Model	WF4M + FFHQ + CelebA	0.5M(10k × 50)	98.81	90.18	91.87	92.63	85.16	91.73	-	-
HyperFace [31] ICLR'25		WF4M + FFHQ + CelebA	0.5M(10k × 50)	98.50	86.53	88.83	89.40	84.23	89.29	-	-
DCFace [24] CVPR'23		FFHQ + C-WF	0.5M(10k × 50)	98.55	89.70	85.33	91.60	82.62	89.56	60.80	74.63
ID ³ [45] NeurIPS'24		C-WF	0.5M(10k × 50)	97.68	91.00	86.84	90.73	82.77	89.80	-	-
CemiFace [41] NeurIPS'24		C-WF	0.5M(10k × 50)	99.03	<u>91.33</u>	91.06	<u>92.42</u>	87.65	92.30	-	-
NegFaceDiff [9] ICCV-W'25		C-WF	0.5M(10k × 50)	98.98	90.02	91.67	91.65	<u>88.82</u>	92.23	77.38	86.11
UIFace [26] ICLR'25		C-WF	0.5M(10k × 50)	<u>99.27</u>	90.95	94.29	92.25	89.58	<u>93.27</u>	<u>81.78*</u>	<u>88.70*</u>
IDPERTURB (Ours)		C-WF	0.5M(10k × 50)	99.40	93.20	<u>93.61</u>	93.50	88.37	93.62	82.28	89.49
DCFace [24] CVPR'23		FFHQ + C-WF	1.2M(20k × 50 + 40k × 5)	98.58	90.97	88.61	92.82	85.07	91.21	-	-
CemiFace [41] NeurIPS'24		C-WF	1.0M(20k × 50)	99.18	91.97	92.75	93.01	88.42	93.07	-	-
Arc2Face [33] ECCV'24	WF4M + FFHQ + CelebA	1.2M(20k × 50 + 40k × 5)	98.92	92.45	94.58	<u>93.33</u>	86.45	93.14	-	-	
UIFace [26] ICLR'25	C-WF	1.0M(20k × 50)	99.22	92.45	95.03	93.18	90.42	<u>94.06</u>	-	-	
IDPERTURB (Ours)	C-WF	1.0M(20k × 50)	99.48	94.03	<u>95.01</u>	93.85	<u>90.01</u>	94.48	85.57	91.19	

thetic IDPERTURB narrows the gap in constrained training settings with an average accuracy of 93.62%. We then generated 1.0M samples using IDPERTURB to train FR and compare to SOTA approaches that generated larger amounts of data to train FR systems. One can notice that IDPERTURB still ranks first with an average accuracy of 94.48%, outperforming SOTA approaches. Evaluations of demographic bias are provided in the supplementary materials.

6. Conclusion

We presented IDPERTURB, a geometry-driven sampling strategy designed for enhancing intra-class variation in identity-conditioned synthetic face generation. Unlike prior works that rely on auxiliary conditions, architectural modifications, or iterative sampling procedures, IDPERTURB perturbs identity embeddings within a constrained angular region of the hyper-sphere to produce diverse yet identity-consistent samples. Through a series of experiments, we show that synthetic datasets generated with IDPERTURB

yield strong performance across both small and large-scale face verification benchmarks, outperforming previous works on most of the considered benchmarks. These results validate the effectiveness of leveraging the geometric structure of identity embeddings to induce diversity in the generated samples, improving the generalizability of FR models without sacrificing semantic coherence.

Limitations Despite its simplicity and effectiveness, IDPERTURB has a few limitations. First, the method does not explicitly control disentangled attributes such as illumination or expression, which may be important for applications beyond FR, e.g., photo editing. Second, IDPERTURB relies on the quality of the underlying DM; any biases or inaccuracies in this model could affect the realism and utility of the generated data. Lastly, while the cosine similarity threshold \mathbf{Ib} offers an interpretable mechanism for diversity control, selecting an appropriate value may require empirical tuning depending on the downstream application.

Acknowledgments

This research work has been funded by the German Federal Ministry of Education and Research and the Hessian Ministry of Higher Education, Research, Science and the Arts within their joint support of the National Research Center for Applied Cybersecurity ATHENE.

References

- [1] Gwangbin Bae, M. D. L. Gorce, Tadas Baltrušaitis, Charlie Hewitt, Dong Chen, Julien P. C. Valentin, Roberto Cipolla, and JingJing Shen. Digiface-1m: 1 million digital face images for face recognition. *2023 IEEE/CVF Winter Conference on Applications of Computer Vision (WACV)*, pages 3515–3524, 2022. 8
- [2] Yuanhao Ban, Ruochen Wang, Tianyi Zhou, Minhao Cheng, Boqing Gong, and Cho-Jui Hsieh. Understanding the impact of negative prompts: When and how do they take effect? In *European Conference on Computer Vision*, pages 190–206. Springer, 2024. 3
- [3] Fadi Boutros, Naser Damer, Florian Kirchbuchner, and Arjan Kuijper. Elasticface: Elastic margin loss for deep face recognition. In *Proceedings of the IEEE/CVF Conference on Computer Vision and Pattern Recognition (CVPR) Workshops*, pages 1578–1587, 2022. 5, 6
- [4] Fadi Boutros, Marco Huber, Patrick Siebke, Tim Rieber, and Naser Damer. Sface: Privacy-friendly and accurate face recognition using synthetic data. *2022 IEEE International Joint Conference on Biometrics (IJCB)*, pages 1–11, 2022. 2, 5, 6, 8
- [5] Fadi Boutros, Jonas Henry Grebe, Arjan Kuijper, and Naser Damer. Idiff-face: Synthetic-based face recognition through fizzy identity-conditioned diffusion models. In *IEEE/CVF International Conference on Computer Vision, ICCV 2023, Paris, France, October 1-6, 2023*, pages 19593–19604. IEEE, 2023. 1, 2, 3, 4, 5, 6, 8
- [6] Fadi Boutros, Marcel Klemm, Meiling Fang, Arjan Kuijper, and Naser Damer. Unsupervised face recognition using unlabeled synthetic data. In *17th IEEE International Conference on Automatic Face and Gesture Recognition, FG 2023, Waikoloa Beach, HI, USA, January 5-8, 2023*, pages 1–8. IEEE, 2023. 2, 8
- [7] Fadi Boutros, Marcel Klemm, Meiling Fang, Arjan Kuijper, and Naser Damer. Exfacegan: Exploring identity directions in gan’s learned latent space for synthetic identity generation. In *IEEE International Joint Conference on Biometrics, IJCB 2023, 2023*. 2, 6, 8
- [8] Fadi Boutros, Marco Huber, Anh Thi Luu, Patrick Siebke, and Naser Damer. Sface2: Synthetic-based face recognition with w-space identity-driven sampling. *IEEE Transactions on Biometrics, Behavior, and Identity Science*, pages 1–1, 2024. 2, 8
- [9] Eduarda Caldeira, Naser Damer, and Fadi Boutros. Neg-facediff: The power of negative context in identity-conditioned diffusion for synthetic face generation. In *Proceedings of the IEEE/CVF International Conference on Computer Vision (ICCV) Workshops*, pages 5914–5924, 2025. 8
- [10] Qiong Cao, Li Shen, Weidi Xie, Omkar M. Parkhi, and Andrew Zisserman. Vggface2: A dataset for recognising faces across pose and age. In *13th IEEE International Conference on Automatic Face & Gesture Recognition, FG 2018, Xi’an, China, May 15-19, 2018*, pages 67–74. IEEE Computer Society, 2018. 1
- [11] Ivan DeAndres-Tame, Ruben Tolosana, Pietro Melzi, Ruben Vera-Rodriguez, Minchul Kim, Christian Rathgeb, Xiaoming Liu, Luis F. Gomez, Aythami Morales, Julian Fierrez, Javier Ortega-Garcia, Zhizhou Zhong, Yuge Huang, Yuxi Mi, Shouhong Ding, Shuigeng Zhou, Shuai He, Lingzhi Fu, Heng Cong, Rongyu Zhang, Zhihong Xiao, Evgeny Smirnov, Anton Pimenov, Aleksei Grigorev, Denis Timoshenko, Kaleb Mesfin Asfaw, Cheng Yaw Low, Hao Liu, Chuyi Wang, Qing Zuo, Zhixiang He, Hatem Otroushi Shahreza, Anjith George, Alexander Unnervik, Parsa Rahimi, Sébastien Marcel, Pedro C. Neto, Marco Huber, Jan Niklas Kolf, Naser Damer, Fadi Boutros, Jaime S. Cardoso, Ana F. Sequeira, Andrea Atzori, Gianni Fenu, Mirko Marras, Vitomir Štruc, Jiang Yu, Zhangjie Li, Jichun Li, Weisong Zhao, Zhen Lei, Xiangyu Zhu, Xiao-Yu Zhang, Bernardo Biesseck, Pedro Vidal, Luiz Coelho, Roger Granada, and David Menotti. Second frcsyn-ongoing: Winning solutions and post-challenge analysis to improve face recognition with synthetic data. *Information Fusion*, page 103099, 2025. 1, 2
- [12] Jiankang Deng, Jia Guo, Jing Yang, Niannan Xue, Irene Kotisa, and Stefanos Zafeiriou. Arcface: Additive angular margin loss for deep face recognition. *IEEE Transactions on Pattern Analysis and Machine Intelligence*, 44(10):5962–5979, 2022. 1, 6
- [13] Yu Deng, Jiaolong Yang, Dong Chen, Fang Wen, and Xin Tong. Disentangled and controllable face image generation via 3d imitative-contrastive learning. In *2020 IEEE/CVF Conference on Computer Vision and Pattern Recognition, CVPR 2020, Seattle, WA, USA, June 13-19, 2020*, pages 5153–5162. Computer Vision Foundation / IEEE, 2020. 2
- [14] César Augusto Fontanillo López and Abdullah Elbi. On synthetic data: a brief introduction for data protection law dummies. <https://europeanlawblog.eu/2022/09/22/on-synthetic-data-a-brief-introduction-for-data-protection-law-dummies/>, 2022. 1
- [15] Yandong Guo, Lei Zhang, Yuxiao Hu, Xiaodong He, and Jianfeng Gao. Ms-celeb-1m: A dataset and benchmark for large-scale face recognition. In *Computer Vision - ECCV 2016 - 14th European Conference, Amsterdam, The Netherlands, October 11-14, 2016, Proceedings, Part III*, pages 87–102. Springer, 2016. 1, 6
- [16] Kaiming He, X. Zhang, Shaoqing Ren, and Jian Sun. Deep residual learning for image recognition. *2016 IEEE Conference on Computer Vision and Pattern Recognition (CVPR)*, pages 770–778, 2015. 6
- [17] Jonathan Ho and Tim Salimans. Classifier-free diffusion guidance. *CoRR*, abs/2207.12598, 2022. 3

- [18] Jonathan Ho, Ajay Jain, and Pieter Abbeel. Denoising diffusion probabilistic models. In *Advances in Neural Information Processing Systems 33: Annual Conference on Neural Information Processing Systems 2020, NeurIPS 2020, December 6-12, 2020, virtual*, 2020. 3
- [19] Gary B. Huang, Manu Ramesh, Tamara Berg, and Erik Learned-Miller. Labeled faces in the wild: A database for studying face recognition in unconstrained environments. Technical Report 07-49, University of Massachusetts, Amherst, 2007. 6
- [20] Kimmo Karkkainen and Jungseock Joo. Fairface: Face attribute dataset for balanced race, gender, and age for bias measurement and mitigation. In *Proceedings of the IEEE/CVF Winter Conference on Applications of Computer Vision*, pages 1548–1558, 2021. 6
- [21] Tero Karras, Samuli Laine, and Timo Aila. A style-based generator architecture for generative adversarial networks. In *IEEE Conference on Computer Vision and Pattern Recognition, CVPR 2019, Long Beach, CA, USA, June 16-20, 2019*, pages 4401–4410. Computer Vision Foundation / IEEE, 2019. 1, 2, 5, 8
- [22] Tero Karras, Miika Aittala, Janne Hellsten, Samuli Laine, Jaakko Lehtinen, and Timo Aila. Training generative adversarial networks with limited data. In *Advances in Neural Information Processing Systems 33: Annual Conference on Neural Information Processing Systems 2020, NeurIPS 2020, December 6-12, 2020, virtual*, 2020. 1, 2
- [23] Minchul Kim, Anil K. Jain, and Xiaoming Liu. Adaface: Quality adaptive margin for face recognition. In *CVPR*, pages 18729–18738. IEEE, 2022. 1, 5, 6
- [24] Minchul Kim, Feng Liu, Anil K. Jain, and Xiaoming Liu. Dcface: Synthetic face generation with dual condition diffusion model. In *IEEE/CVF Conference on Computer Vision and Pattern Recognition, CVPR 2023, Vancouver, BC, Canada, June 17-24, 2023*, pages 12715–12725. IEEE, 2023. 1, 2, 3, 8
- [25] Jan Niklas Kolf, Tim Rieber, Jurek Elliesen, Fadi Boutros, Arjan Kuijper, and Naser Damer. Identity-driven three-player generative adversarial network for synthetic-based face recognition. In *IEEE/CVF Conference on Computer Vision and Pattern Recognition, CVPR 2023 - Workshops, Vancouver, BC, Canada, June 17-24, 2023*, pages 806–816. IEEE, 2023. 2, 8
- [26] Xiao Lin, Yuge Huang, Jianqing Xu, Yuxi Mi, Shuigeng Zhou, and Shouhong Ding. Uiface: Unleashing inherent model capabilities to enhance intra-class diversity in synthetic face recognition. In *ICLR*. OpenReview.net, 2025. 1, 2, 3, 4, 5, 6, 8
- [27] Brianna Maze, Jocelyn C. Adams, James A. Duncan, Nathan D. Kalka, Tim Miller, Charles Otto, Anil K. Jain, W. Tyler Niggel, Janet Anderson, Jordan Cheney, and Patrick Grother. IARPA janus benchmark - C: face dataset and protocol. In *ICB*, pages 158–165. IEEE, 2018. 6, 8
- [28] Pietro Melzi, Christian Rathgeb, Ruben Tolosana, Rubén Vera-Rodríguez, Dominik Lawatsch, Florian Domin, and Maxim Schaubert. Gandifface: Controllable generation of synthetic datasets for face recognition with realistic variations. In *IEEE/CVF International Conference on Computer Vision, ICCV 2023 - Workshops, Paris, France, October 2-6, 2023*, pages 3078–3087. IEEE, 2023. 2
- [29] Pietro Melzi, Ruben Tolosana, Rubén Vera-Rodríguez, Minchul Kim, Christian Rathgeb, Xiaoming Liu, Ivan DeAndres-Tame, Aythami Morales, Julian Fierrez, Javier Ortega-Garcia, Weisong Zhao, Xiangyu Zhu, Zheyu Yan, Xiaoyu Zhang, Jinlin Wu, Zhen Lei, Suvidha Tripathi, Mahak Kothari, Md Haider Zama, Debayan Deb, Bernardo Biesseck, Pedro Vidal, Roger Granada, Guilherme P. Fickel, Gustavo Führ, David Menotti, Alexander Unnervik, Anjith George, Christophe Ecabert, Hatf Otroshi-Shahreza, Parsa Rahimi, Sébastien Marcel, Ioannis Sarridis, Christos Koutlis, Georgia Baltsou, Symeon Papadopoulos, Christos Diou, Nicolò Di Domenico, Guido Borghi, Lorenzo Pellegrini, Enrique Mas-Candela, Ángela Sánchez-Pérez, Andrea Atzori, Fadi Boutros, Naser Damer, Gianni Fenu, and Mirko Marras. Fracsyn-ongoing: Benchmarking and comprehensive evaluation of real and synthetic data to improve face recognition systems. *Inf. Fusion*, 107:102322, 2024. 1, 2
- [30] Stylianos Moschoglou, Athanasios Papaioannou, Christos Sagonas, Jiankang Deng, Irene Kotsia, and Stefanos Zafeiriou. Agedb: The first manually collected, in-the-wild age database. In *2017 IEEE Conference on Computer Vision and Pattern Recognition Workshops (CVPRW)*, pages 1997–2005, 2017. 6
- [31] Hatf Otroshi-Shahreza and Sébastien Marcel. Hyperface: Generating synthetic face recognition datasets by exploring face embedding hypersphere. In *ICLR*. OpenReview.net, 2025. 1, 2, 3, 8
- [32] Hatf Otroshi-Shahreza, Christophe Ecabert, Anjith George, Alexander Unnervik, Sébastien Marcel, Nicolò Di Domenico, Guido Borghi, Davide Maltoni, Fadi Boutros, Julia Vogel, Naser Damer, Ángela Sánchez-Pérez, Enrique Mas-Candela, Jorge Calvo-Zaragoza, Bernardo Biesseck, Pedro Vidal, Roger Granada, David Menotti, Ivan DeAndres-Tame, Simone Maurizio La Cava, Sara Concas, Pietro Melzi, Ruben Tolosana, Rubén Vera-Rodríguez, Gianpaolo Perelli, Giulia Orrù, Gian Luca Marcialis, and Julian Fierrez. SDFR: synthetic data for face recognition competition. In *FG*, pages 1–9. IEEE, 2024. 1, 2
- [33] Foivos Paraperas Papantoniou, Alexandros Lattas, Stylianos Moschoglou, Jiankang Deng, Bernhard Kainz, and Stefanos Zafeiriou. Arc2face: A foundation model for id-consistent human faces. In *ECCV (37)*, pages 241–261. Springer, 2024. 1, 2, 8
- [34] Norman Poh and Samy Bengio. A study of the effects of score normalisation prior to fusion in biometric authentication tasks. Technical report, IDIAP, 2004. 5
- [35] Haibo Qiu, Baosheng Yu, Dihong Gong, Zhifeng Li, Wei Liu, and Dacheng Tao. Synface: Face recognition with synthetic data. In *2021 IEEE/CVF International Conference on Computer Vision, ICCV 2021, Montreal, QC, Canada, October 10-17, 2021*, pages 10860–10870. IEEE, 2021. 2, 8
- [36] Robin Rombach, A. Blattmann, Dominik Lorenz, Patrick Esser, and Björn Ommer. High-resolution image synthesis with latent diffusion models. *2022 IEEE/CVF Conference on Computer Vision and Pattern Recognition (CVPR)*, pages 10674–10685, 2021. 1, 2, 3, 5

- [37] Nataniel Ruiz, Eunji Chong, and James M. Rehg. Fine-grained head pose estimation without keypoints. In *The IEEE Conference on Computer Vision and Pattern Recognition (CVPR) Workshops*, 2018. 6
- [38] Soumyadip Sengupta, Jun-Cheng Chen, Carlos Domingo Castillo, Vishal M. Patel, Rama Chellappa, and David W. Jacobs. Frontal to profile face verification in the wild. *2016 IEEE Winter Conference on Applications of Computer Vision (WACV)*, pages 1–9, 2016. 6
- [39] Henrique Siqueira, Sven Magg, and Stefan Wermter. Efficient facial feature learning with wide ensemble-based convolutional neural networks. In *The Thirty-Fourth AAAI Conference on Artificial Intelligence (AAAI-20)*, pages 1–1, 2020. 6
- [40] Jiaming Song, Chenlin Meng, and Stefano Ermon. Denoising diffusion implicit models. In *ICLR*. OpenReview.net, 2021. 5
- [41] Zhonglin Sun, Siyang Song, Ioannis Patras, and Georgios Tzimiropoulos. Cemiface: Center-based semi-hard synthetic face generation for face recognition. In *NeurIPS*, 2024. 5, 6, 8
- [42] The European Parliament and the Council of the European Union. General data protection regulation, 2016. 1
- [43] Hao Wang, Yitong Wang, Zheng Zhou, Xing Ji, Dihong Gong, Jingchao Zhou, Zhifeng Li, and Wei Liu. Cosface: Large margin cosine loss for deep face recognition. In *CVPR*, pages 5265–5274. Computer Vision Foundation / IEEE Computer Society, 2018. 1, 6
- [44] Ruochen Wang, Ting Liu, Cho-Jui Hsieh, and Boqing Gong. On discrete prompt optimization for diffusion models. In *ICML*. OpenReview.net, 2024. 3
- [45] Jianqing Xu, Shen Li, Jiaying Wu, Miao Xiong, Ailin Deng, Jiazhen Ji, Yuge Huang, Guodong Mu, Wenjie Feng, Shouhong Ding, and Bryan Hooi. Id³: Identity-preserving-yet-diversified diffusion models for synthetic face recognition. In *NeurIPS*, 2024. 1, 2, 3, 8
- [46] Dong Yi, Zhen Lei, Shengcai Liao, and Stan Z. Li. Learning face representation from scratch. *CoRR*, abs/1411.7923, 2014. 5, 8
- [47] Richard Zhang, Phillip Isola, Alexei A. Efros, Eli Shechtman, and Oliver Wang. The unreasonable effectiveness of deep features as a perceptual metric. In *CVPR*, pages 586–595. Computer Vision Foundation / IEEE Computer Society, 2018. 6
- [48] Tianyue Zheng and Weihong Deng. Cross-pose lfw : A database for studying cross-pose face recognition in unconstrained environments. 2018. 6
- [49] Tianyue Zheng, Weihong Deng, and Jiani Hu. Cross-age lfw: A database for studying cross-age face recognition in unconstrained environments. 2017. 6
- [50] Zheng Zhu, Guan Huang, Jiankang Deng, Yun Ye, Junjie Huang, Xinze Chen, Jiagang Zhu, Tian Yang, Jiwen Lu, Dalong Du, and Jie Zhou. Webface260m: A benchmark unveiling the power of million-scale deep face recognition. In *CVPR*, pages 10492–10502. Computer Vision Foundation / IEEE, 2021. 2, 8